JOURNAL OF CATALYSIS **173,** 304–314 (1998)
ARTICLE NO. CA971932

Kinetics of the NO and CO Reaction over Platinum Catalysts

I. Influence of the Support

P. Granger, C. Dathy, J. J. Lecomte, L. Leclercq, M. Prigent,* G. Mabilon,* and G. Leclercq[1]

*Université des Sciences et Technologies de Lille I, URA-CNRS 0402, Bât. C3, 59655-Villeneuve d'Ascq Cedex, France; and *Institut Français du Pétrole, 1 et 4 avenue de Bois-Préau, B.P. 311, 92506-Rueil-Malmaison Cedex, France*

Received February 5, 1997; revised July 10, 1997; accepted September 25, 1997

The kinetics of the CO + NO reaction over Pt-based catalysts was investigated using a fixed bed flow reactor at 300°C, with CO and NO partial pressure ranges of 1.5×10^{-3} to 9×10^{-3} atm. Pt was deposited on various supports: γ-Al_2O_3, Si_3N_4, and Cr_3C_2. XRD, XPS, and hydrogen chemisorption measurements seem to indicate that Pt dispersion decreases as follows: $Pt/Al_2O_3 > Pt/Si_3N_4 > Pt/Cr_3C_2$. Kinetic data obtained on these Pt catalysts were interpreted on the basis of four mechanisms as proposed in the literature; only one mechanism can correctly model the reactant partial pressure dependencies of the rate. This mechanism involves nondissociative CO and NO competitive adsorptions followed by a dissociation of adsorbed NO which requires a vacant nearest-neighbor adsorption site. Clearly, the adsorption equilibrium constants, λ_{CO} and λ_{NO} of CO and NO, together with the rate constant of the NO dissociation step are strongly influenced by the support, particularly λ_{NO}, which is consistently lower than λ_{CO} on Pt/Al_2O_3, increases notably for Pt/Si_3N_4, and increases even more for Pt/Cr_3C_2. It has been shown that Pt/Si_3N_4 may be the most suitable catalyst if the Pt dispersion on this support can be improved. The nature of the support also has a significant effect on the selectivity of the NO transformation into N_2 and N_2O. Pt/Cr_3C_2 is the most selective catalyst for N_2 formation (much more than Pt/Si_3N_4 and particularly Pt/Al_2O_3). This seems to be related to the fact that the rate constant of the step $2N_{ads} \rightarrow N_2$ is much higher than that of the other step $N_{ads} + NO_{ads} \rightarrow N_2O$.

INTRODUCTION

Platinum and rhodium are widely used in three-way catalytic converters (TWCs) because of their efficiency in transforming NO and CO simultaneously (1–4) with respect to the following reactions:

$$2CO + 2NO \rightarrow N_2 + 2CO_2 \quad [1]$$

$$CO + 2NO \rightarrow N_2O + CO_2 \quad [2]$$

$$CO + N_2O \rightarrow N_2 + CO_2. \quad [3]$$

Numerous studies have reported that the addition of rhodium to platinum has a beneficial effect on the activity and selectivity of three-way catalysts in the CO + NO reaction. Such an enhancement has been assigned to the greater ability of metallic Rh to dissociate NO as compared to that of Pt. Despite the crucial role of Rh in postcombustion catalysis, the substitution of rhodium and/or platinum for less expensive metals is of greatest importance because it would considerably lower the cost of TWCs. The work of Gandhi *et al.* (5) and Plummer *et al.* (6) are relevant, because these authors have shown that $Pt(Pd)/MoO_x(WO_x)$ exhibits properties similar to those of conventional three-way catalysts. Unfortunately the severe deactivation of this catalyst under the actual operating conditions of a TWC limits its industrial development. Nevertheless, the replacement or at least the reduction of noble metals, in particular Rh, is still an important goal and has been explored in our laboratory.

In a preliminary study on the role of metal–support interaction as a key element of the operating mode of TWCs (7, 8), we reported the catalytic properties of Pt supported on various nonclassical supports in the reaction CO + NO ($+O_2$). These supports are mainly carbides and nitrides of noble transition metals, selected among those more resistant to oxidation, since these solids must be used under oxidizing conditions. Among the numerous supports used, two proved interesting: Cr_3C_2 and Si_3N_4. The pure supports were active in the CO + NO reaction but to a lesser extent than Pt/Al_2O_3. However, a synergistic effect between Pt and Si_3N_4 was proven, since Pt/Si_3N_4 is significantly more active than Pt/Al_2O_3, and Pt/Cr_3C_2 was only slightly more active than Pt/Al_2O_3. Moreover, a better selectivity was observed on these two catalysts, particularly on Pt/Cr_3C_2, since N_2O production was significantly lower than on Pt/Al_2O_3 and other TWCs. In addition, these two supports do not oxidize to the same extent as those mentioned in Ref. (7), since bulk oxidation only occurs at 650°C for Cr_3C_2 and at more than 1100°C for Si_3N_4. XPS measurements detected only silicon nitride on Pt/Si_3N_4, hence no oxidation, even after several catalytic cycles with oxygen in the feed.

[1] To whom correspondence should be addressed.

0021-9517/98 $25.00

It seemed to be an interesting challenge to understand the reasons for the improvement of the catalytic properties of platinum. Our contribution to explaining the influence of Cr_3C_2 and Si_3N_4 on the activity and selectivity of Pt in the CO + NO reaction is based on a detailed kinetic study. The purpose of this study was first to select a mechanism able to describe the CO oxidation by NO on Pt (this mechanism will be further used to study the influence of Rh addition on Pt activity in our next experiment in this series and then to use the rate equation derived from the selected mechanism to calculate the parameters corresponding to the various steps on Pt deposited on Al_2O_3, Si_3N_4, and Cr_3C_2 in order to assess the influence of the support on these parameters and to explain the different catalytic performances. Modifications of Pt catalytic behavior with the support are still being debated on the basis of two general concepts. It is well known that the adsorption properties of metals in interaction with the support with a second metal can be discussed in terms of electronic modifications of all surface atoms, as suggested by Ng *et al.* (9), or in terms of geometric effects, as mentioned by Oh and Eickel (10).

EXPERIMENTAL

1. Catalyst Preparation and Characterization

The supports used were γ-Al_2O_3 (100 $m^2\,g^{-1}$), Si_3N_4 (12.5 $m^2\,g^{-1}$, "Ceramique et Composite"), and Cr_3C_2 (<1 $m^2\,g^{-1}$, "Metabap"). These materials were impregnated with aqueous or methanolic solutions of hexachloroplatinic acid to obtain 1 wt% Pt loading. Then the precursor was dried at 120°C. Only Pt/Al_2O_3 was submitted to a reduction step in flowing hydrogen at 500°C for 2 h during preparation. The physical and chemical characterizations were performed by X-ray photoelectron spectroscopy (XPS) with a Leybold Heraeus LHS10 spectrometer. The Pt energy level was referenced to Al 2*p* (74.6 eV) for Pt/Al_2O_3 and to C1*s* (285 eV) for Pt/Cr_3C_2 and Pt/Si_3N_4. X-ray diffraction (XRD) measurements were carried out in a Siemens D5000 spectrometer using Cu$K\alpha$ radiation (0.15418 nm). Hydrogen chemisorption measurements were performed in a classical volumetric apparatus described in Ref. (11). The metal dispersion was calculated by extrapolation to zero pressure of the hydrogen adsorption isotherm (pressure range 6×10^{-2} to 0.3 atm) (1 atm $\cong 10^5$ Pa).

2. Catalyst Testing

The catalytic experiments were carried out in a fixed bed flow reactor at atmospheric pressure (global flow rate 10 liters h^{-1}, 0.2 g catalyst mixed with 0.8 g α-Al_2O_3). The catalyst samples were reduced in situ in flowing hydrogen (3 liters h^{-1}) at 500°C for 7 h and then cooled to room temperature. The reactants were diluted in helium, and flow rates were adjusted by means of Brooks mass flow meters (model 5850 TR). The partial pressure ranges were 1.5×10^{-3} to 5.6×10^{-3} atm for the NO partial pressure (P_{NO}) and 5×10^{-3} to 9×10^{-3} atm for the CO partial pressure (P_{CO}). The inlet and outlet gas mixtures were analyzed by means of a chromatograph (HP5890 series II) equipped with a thermal conductivity detector. The components were separated at 30°C on a CTR1 column (Alltech) which consists of two concentric columns, the inner one of which is filled with a molecular sieve of 0.5 nm (for NO, CO, and N_2 separation) and the outer with porapack Q (for N_2O and CO_2 separation). The initial conversions (at zero time) were determined according to the procedure described in Refs. (12) and (13).

RESULTS AND DISCUSSION

1. Catalyst Characterization

The results of the physicochemical characterization of the Pt catalysts are summarized in Table 1.

The first point to be noted is the low capacity of Pt/Si_3N_4 and Pt/Cr_3C_2 to chemisorb hydrogen in comparison with Pt/Al_2O_3. This phenomenon may be related either to low Pt dispersion on Si_3N_4 and Cr_3C_2 or to incomplete Pt reduction. However, XPS results with a binding energy (B.E.) for Pt $4f_{7/2}$ and Pt $4f_{5/2}$ levels close to 71 and 74 eV on both Pt/Si_3N_4 and Pt/Cr_3C_2, taking into account the high margin of error because of the low Pt contents, seem to be consistent with the presence of Pt. Hence the low H_2 uptakes on the catalysts deposited on Si_3N_4 and Cr_3C_2 are probably due to larger Pt particles, which is understandable if we consider the low surface areas of these two supports. In the same way, the B.E. of Pt $4d_{5/2}$ and Pt $4d_{3/2}$ levels at 315.3 and 331.8 eV, close to values usually reported for Pt metal on Pt/Al_2O_3 (14), indicate the complete reduction of the Pt precursor.

The observed XPS intensity I_{Pt}/I_M ratio (M = Al, Si, Cr) of the Pt dispersed phase was used to estimate the particle size, d_{Pt}, of Pt (15, 16) according to a simple procedure described in Appendix. I. The model used to calculate the average size, d_{Pt}, of the supported particles assumes that

TABLE 1

Characterization of Supported Pt Catalysts

Catalyst	Specific surface area ($m^2\,g^{-1}$)	Metal dispersion (%)	XPS analysis: B.E. (eV) Pt $4f_{7/2}$	Pt $f_{5/2}$	I_{Pt}/I_M[a]	d_{Pt}[b] (nm)
Pt/Al_2O_3	100	55	n.m.	n.m.	4.07×10^{-2}	1.0
Pt/Cr_3C_2	<1	Very low	71	74.3	1.02	70
Pt/Si_3N_4	12.5	Very low	71.8	75	0.154	7.5

[a] Relative intensity of Pt XPS peak: (M = Al, Cr, or Si).
[b] Edge of cubic particle of Pt.

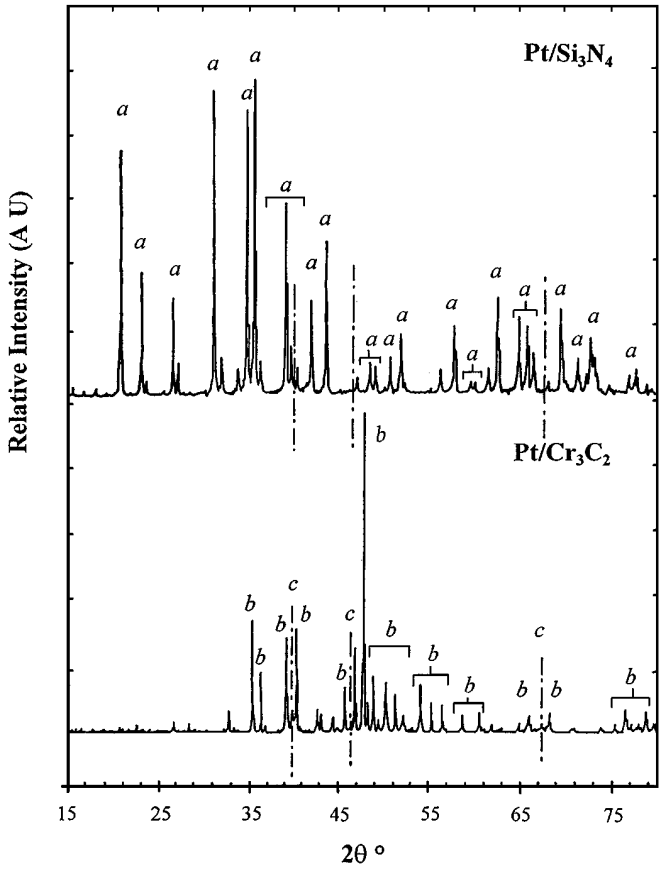

FIG. 1. XRD diffractograms for Pt catalysts. (a) Si_3N_4; (b) Cr_3C_2; (c) Pt.

these particles are cubic with d_{Pt} corresponding to the edge of the cubic particles. The results obtained from this simple calculation are reported in Table 1. It is noteworthy that d_{Pt} close to 1 nm for Pt/Al_2O_3 corresponds to a Pt dispersion of ~100%, which differs from that calculated from hydrogen chemisorption (55%). This is probably related to the model which considers that the support is nonporous. This is probably an oversimplification for Al_2O_3. Of course, these values give only a rough idea of the changes of the metal particle sizes on the various supports, but they are in agreement with hydrogen chemisorption. X-ray diffraction measurements reported in Fig. 1 support this assumption since X-ray detectable Pt bulk species are observed only on Pt/Cr_3C_2. The trends observed from examining these different experimental data suggest that the metal dispersion is largely influenced by the specific surface area of the support. We propose the following sequence where the platinum dispersion decreases in the order $Pt/Al_2O_3 > Pt/Si_3N_4 > Pt/Cr_3C_2$.

2. Kinetics of the CO + NO Reaction

2.1. Catalyst Deactivation

A preliminary study was performed by reacting a mixture containing NO and CO diluted in helium under the following reference pressure conditions: $P_{NO} = 5.6 \times 10^{-3}$ atm, $P_{CO} = 5 \times 10^{-3}$ atm. CO_2, N_2, and N_2O are primary products, as mentioned by Cho *et al.* (17). According to reaction steps [1] to [3], the conversion of CO with NO (T_{1CO}) is given by

$$T_{1CO} = T_{N_2} + \frac{T_{N_2O}}{2}. \quad [4]$$

The changes of the overall CO (T_{CO}) and NO (T_{NO}) conversions on the Pt/Al_2O_3 catalyst at 303°C versus time on stream are shown in Fig. 2. The curve for the first run shows two conversion regimes. First, a significant decrease in the CO and NO conversions occurs at the beginning of the reaction. Then, after about 3 h, NO and CO conversions become stabilized. When the steady state is achieved, one reaction parameters (temperature or reactant partial pressure) is modified; after several hours under these conditions another change in the reaction parameters takes place. Finally, at the end of the experiments, the initial experimental conditions are applied again to prove deactivation. Slight decreases in the CO and NO conversions are observed at the end of the reaction when the catalyst runs under operating conditions similar to those selected at the beginning of the reaction. This slight deactivation, which operates at steady state on Pt/Al_2O_3, appears to affect the transformation of CO to a greater extent that than of NO.

An unexpected feature was found: while deactivation proceeds, T_{NO} (which should always be higher than or equal to T_{CO} according to the stoichiometry of the reactions leading to the formation of N_2 or of N_2O) is lower than T_{CO}. Consequently, the values calculated for T_{1CO}, the conversion of CO oxidation by NO, are always lower than those for T_{CO}, the global CO conversion. These observations prove the occurrence of an additional process for CO conversion, the contribution of which can be estimated according to

$$T'_{CO} = T_{CO} - T_{1CO}. \quad [5]$$

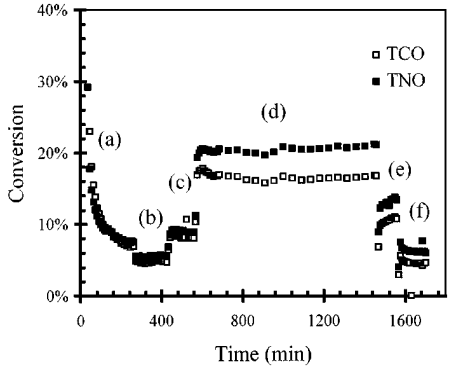

FIG. 2. Influence of the temperature on the overall conversion of NO and CO on Pt/Al_2O_3 ($P_{NO} = 5.6 \times 10^{-3}$ atm, $P_{CO} = 5 \times 10^{-3}$ atm) at various temperatures: (a) 303°C; (b) 292°C; (c) 311°C; (d) 333°C; (e) 325°C; (f) 300°C.

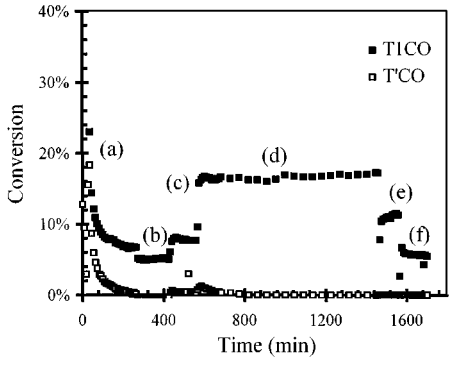

FIG. 3. CO conversion vs time at various temperatures. T_{1CO}, CO conversion by reaction with NO; T'_{CO}, CO conversion by the extra process for CO_2 formation ($P_{NO} = 5.6 \times 10^{-3}$ atm, $P_{CO} = 5 \times 10^{-3}$ atm) at various temperatures: (a) 303°C; (b) 292°C; (c) 311°C; (d) 333°C; (e) 325°C; (f) 300°C.

The plots to T'_{CO} and T_{1CO} versus time in Fig. 3 show the disappearance of the additional process at steady state.

Figure 4 illustrates the initial deactivation on Pt/Al_2O_3, Pt/Cr_3C_2, and Pt/Si_3N_4 at 300°C ($P_{NO} = 5.6 \times 10^{-3}$ atm, $P_{CO} = 5 \times 10^{-3}$ atm). Pt/Al_2O_3 obviously deactivates more readily than Pt/Si_3N_4 and, in particular, Pt/Cr_3C_2. The origin of deactivation cannot be identified with certainty. Nevertheless, one can argue about the stability of Pt catalysts on the basis of the following: (i) the loss of activity is observable mainly on well-dispersed catalysts such as Pt/Al_2O_3; (ii) the poorer the dispersion, the higher the catalyst stability; and (iii) while deactivation proceeds, the extra process of CO conversion disappears. Similar deactivation and additional CO transformation were observed by Lorimer and Bell (18) on Pt/SiO_2 and more recently by Mergler and Nieuwenhuys (19) on Pt/Al_2O_3. In fact, the former authors ascribed the additional pathway for CO_2 production, under reducing conditions, to a reaction between one NO molecule and two CO molecules, yielding one CO_2 molecule and one NCO species. NCO groups are primarily formed on metal particles which then migrate rapidly to the support. Nevertheless, NCO species bonded to Pt were also detected from IR measurements (20). Lorimer and Bell (18) thought that the accumulation of NCO groups in the immediate vicinity of platinum particles could alter their electronic properties and subsequently their activity. Deactivation by isocyanate species may explain the lower deactivation of Pt/Si_3N_4 and Pt/Cr_3C_2 since the dispersion of Pt is lower on these two supports. As a matter of fact, since these NCO species on the support are supposed to deactivate the neighboring Pt atoms by electronic modifications, deactivation must be related to the number of Pt atoms at the edge of the support compared to the total number of Pt atoms, i.e., to the Pt dispersion. An alternative explanation has been proposed by Mergler and Nieuwenhuys (19). Although these authors have detected isocyanate species, they suggest that the buildup of strongly adsorbed CO on Pt^{n+} can further block free adsorption sites essential for the dissociation of NO. These authors also suggested that well-dispersed catalysts are more sensitive to deactivation. Despite the discrepancy in the interpretation of deactivation it is expected that the lower the Pt dispersion, the lower the deactivation, which is what we observed for our Pt catalysts. Both authors agree that the adsorption properties of Pt are modified during deactivation.

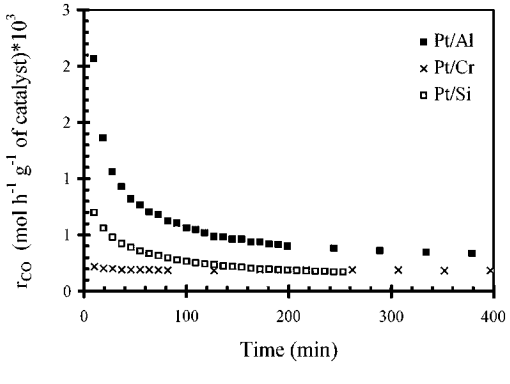

FIG. 4. Deactivation on Pt/Al_2O_3, Pt/Si_3N_4, Pt/Cr_3C_2 – $T = 300$°C, $P_{NO} = 5 \times 10^{-3}$ atm, $P_{CO} = 5 \times 10^{-3}$ atm.

2.2. Formal Kinetics

Effect of the temperature. The apparent activation energies (E) for CO and NO transformation and for N_2 and N_2O formation are given in Table 2. E values associated both with the oxidation process of CO to CO_2 and with the NO transformation N_2 and N_2O vary significantly, in the temperature range studied, for all the catalysts. Hence the increasing values of the apparent activation energies for CO oxidation, according to the sequence $Pt/Al_2O_3 < Pt/Si_3N_4 < Pt/Cr_3C_2$, suggest that this reaction is probably sensitive to changes in catalyst surface properties. Note that the E values on Pt/Al_2O_3 and Pt/Si_3N_4, corresponding to the reduction of NO to N_2, are similar when the uncertainties about the extrapolated conversions are taken into account and significantly lower than those

TABLE 2

CO + NO Reactions over Pt Catalysts ($P_{CO} = 5 \times 10^{-3}$ atm and $P_{NO} = 5.6 \times 10^{-3}$ atm)

Catalyst	Activation energies (kcal mol^{-1})			
	CO[a]	NO[a]	N_2O[b]	N_2[b]
Pt/Al_2O_3	19	22	27	15
Pt/Si_3N_4	26	21	35	11
Pt/Cr_3C_2	34	36	39	32

[a] Apparent activation energy for CO and NO conversion.
[b] Apparent activation energy for N_2O and N_2 formation.

TABLE 3

Influence of the Partial Pressures of Reactants on the Activity and Selectivity of Pt/Si_3N_4 in the CO + NO Reaction

P_{NO} (atm)	P_{CO} (atm)	Conv. (%)	Rate (mol g^{-1} h^{-1}) $\times 10^4$		r_{N_2}/r_{N_2O}	Selectivity (%) S_{N_2O}
			r_{NO}	r		
5×10^{-3}	4.97×10^{-3}	1.18	1.81	1.20	0.48	67.6
5×10^{-3}	6.10×10^{-3}	0.93	1.70	1.16	0.57	63.7
5×10^{-3}	6.93×10^{-3}	0.64	1.35	0.91	0.55	64.5
5×10^{-3}	7.87×10^{-3}	0.57	1.32	0.92	0.68	59.5
5×10^{-3}	9.05×10^{-3}	0.45	1.18	0.83	0.68	59.5
1.48×10^{-3}	5×10^{-3}	0.43	0.57	0.44	1.16	46.2
2.48×10^{-3}	5×10^{-3}	0.69	0.95	0.71	0.95	51.3
3.43×10^{-3}	5×10^{-3}	0.86	1.25	0.88	0.70	58.8
4.49×10^{-3}	5×10^{-3}	1.02	1.53	1.05	0.60	62.5
4.75×10^{-3}	5×10^{-3}	1.11	1.69	1.14	0.53	65.3
4.96×10^{-3}	5×10^{-3}	1.14	1.77	1.17	0.48	67.6
5.53×10^{-3}	5×10^{-3}	1.38	2.13	1.41	0.49	67.1

Note. $T = 300°C$; 0.2 g catalyst; global flow rate = 10 liters h^{-1}.

TABLE 5

Influence of the Partial Pressures of Reactants on the Activity and Selectivity of Pt/Cr_3C_2 in the CO + NO Reaction

P_{NO} (atm)	P_{CO} (atm)	Conv. (%)	Rate (mol g^{-1} h^{-1}) $\times 10^4$		r_{N_2}/r_{N_2O}	Selectivity (%) S_{N_2O}
			r_{NO}	r		
5×10^{-3}	4.99×10^{-3}	0.93	1.22	0.95	1.28	43.9
5×10^{-3}	6.07×10^{-3}	0.67	1.07	0.83	1.22	45
5×10^{-3}	7.05×10^{-3}	0.52	0.96	0.75	1.29	43.7
5×10^{-3}	8×10^{-3}	0.39	0.83	0.64	1.17	46.1
5×10^{-3}	9.11×10^{-3}	0.29	0.71	0.55	1.19	45.7
4.98×10^{-3}	5×10^{-3}	0.89	1.16	0.91	1.28	43.9
1.52×10^{-3}	5×10^{-3}	0.48	0.57	0.49	2.60	27.8
3.47×10^{-3}	5×10^{-3}	0.70	0.90	0.72	1.51	39.8
4.5×10^{-3}	5×10^{-3}	0.78	1.03	0.80	1.24	44.6
4.97×10^{-3}	5×10^{-3}	0.87	1.15	0.89	1.24	44.6
5.58×10^{-3}	5×10^{-3}	1.02	1.34	1.05	1.31	43.3
5.10×10^{-3}	5×10^{-3}	0.96	1.18	0.98	1.20	45.4

Note. $T = 300°C$; 0.2 g catalyst; global flow rate = 10 liters h^{-1}.

measured on Pt/Cr_3C_2. This latter observation may predict an enhancement of N_2 production at high temperature on Pt/Cr_3C_2.

NO and CO partial pressure dependencies of the reaction rates. The activity measurements obtained on Pt/Al_2O_3, Pt/Si_3N_4, and Pt/Cr_3C_2 were performed at 300°C. Two sets of experiments were carried out by varying NO pressure from 1.5×10^{-3} to 5.6×10^{-3} atm and CO pressure from 5×10^{-3} to 9×10^{-3} atm, while CO and NO were maintained at a constant value of 5×10^{-3} atm. The rates, r, of CO oxidation by NO are listed in Tables 3 to 5. The apparent reaction orders obtained from these data by linear regression analysis with respect to the power law expression of the type

$$r = k P_{NO}^{m} P_{CO}^{n} \quad [6]$$

are reported in Table 6.

TABLE 4

Influence of the Partial Pressures of Reactants on the Activity and Selectivity of Pt/Al_2O_3 in the CO + NO Reactions

P_{NO} (atm)	P_{CO} (atm)	Conv. (%)	Rate (mol g^{-1} h^{-1}) $\times 10^4$		r_{N_2}/r_{N_2O}	Selectivity (%) S_{N_2O}
			r_{NO}	r		
5×10^{-3}	5×10^{-3}	2.25	3.62	2.30	0.37	73
5×10^{-3}	6×10^{-3}	1.71	3.31	2.11	0.38	72.5
5×10^{-3}	7×10^{-3}	1.14	2.65	1.64	0.31	76.3
5×10^{-3}	8×10^{-3}	1.00	2.63	1.64	0.33	75.2
5×10^{-3}	9×10^{-3}	0.76	2.30	1.40	0.28	78
1.49×10^{-3}	5×10^{-3}	0.71	1.07	0.72	0.55	64.5
2.49×10^{-3}	5×10^{-3}	1.16	1.81	1.19	0.46	68.5
3.49×10^{-3}	5×10^{-3}	1.60	2.52	1.64	0.43	70
5.03×10^{-3}	5×10^{-3}	2.24	3.53	2.30	0.43	70

Note. $T = 300°C$; 0.2 g catalyst; global flow rate = 10 liters h^{-1}.

In each case, positive values for NO orders are obtained. On the contrary, the CO apparent orders are negative. It is difficult to compare these experimental orders with those reported in the literature by several investigators, since the dependence of the rate on the CO and NO concentrations is widely influenced by the nature of the metal (18, 21) and by the experimental conditions (22) (temperature, reactant pressure ranges). Lorimer and Bell (18) reported a first order in NO and a negative second order in CO on silica-supported platinum under reducing conditions at CO and NO pressures higher than those used in this study (NO varying from 2.6×10^{-2} to 5.5×10^{-2} atm and CO from 3.5×10^{-2} to 10^{-1} atm). Under our experimental conditions, the negative CO order proves the well-known CO-inhibiting effect on the reaction rate. On the other hand, the NO order close to one on Pt/Al_2O_3 suggests a weak adsorption of NO on platinum dispersed on γ-Al_2O_3 compared to that of CO.

TABLE 6

Apparent Orders for the CO + NO Reactions on Pt Catalysts

Catalyst	P_{CO} (atm)	P_{NO} (atm)	m^a	n^a
Pt/Al_2O_3	5×10^{-3}–9×10^{-3}	1.5×10^{-3}–5.6×10^{-3}	0.95	−0.84
Pt/Si_3N_4	5×10^{-3}–9×10^{-3}	1.5×10^{-3}–5.6×10^{-3}	0.80	−0.64
Pt/Cr_3C_2	5×10^{-3}–9×10^{-3}	1.5×10^{-3}–5.6×10^{-3}	0.60	−0.85

[a] Rate = $k \times P_{NO}^{m} \times P_{CO}^{n}$.

MECHANISM 1 (26)

[7]	CO + *	⇔	CO*
[8]	NO + *	⇔	NO*
[9]	CO* + NO*	→	CO_2 + N* + *
[10]	N* + N*	→	N_2 + 2*
[11]	N* + NO*	→	N_2 + O* + *
[12]	N* + NO*	→	N_2O + 2*
[13]	O* + CO*	→	CO_2 + 2*

MECHANISM 2 (17, 27)

[7]	CO + *	⇔	CO*
[8]	NO + *	⇔	NO*
[14]	2 NO*	→	N_2 + 2 O*
[15]	2 NO*	→	N_2O + O* + *
[13]	O* + CO*	→	CO_2 + 2*

MECHANISM 3 (18, 28)

[7]	CO + *	⇔	CO*
[8]	NO + *	⇔	NO*
[16]	NO* + *	→	N* + O*
[10]	N* + N*	→	N_2 + 2*
[11]	N* + NO*	→	N_2 + O* + *
[12]	N* + NO*	→	N_2O + 2*
[13]	O* + CO*	→	CO_2 + 2*

MECHANISM 4

[7]	CO + *	⇔	CO*
[8]	NO + *	⇔	NO*
[17]	NO*	→	[N---------O] ≡ A* (N bonded to *, O bonded to *)
[18]	A* + A*	→	N_2 + 2 O*
[19]	A* + NO*	→	N_2O+ * + O*
[13]	O* + CO*	→	CO_2 + 2*

FIG. 5. Mechanism schemes for the CO + NO reaction on noble metals.

2.3. Mechanisms of CO Transformation

Surface chemistry reaction modeling. The kinetics of the CO + NO reaction were investigated extensively under transient conditions (17, 23) or at steady state (24) over single crystals or supported metal catalysts at various temperatures and various pressures (25). Several mechanism schemes were proposed in the literature to describe the transformation of CO to CO_2 and NO to N_2O and N_2, assuming a Langmuir–Hinshelwood-type mechanism.

We considered the following four mechanisms represented in Fig. 5. These four mechanisms have a nondissociative adsorption of CO and NO on a single adsorption site in common according to Eqs. [7] and [8]. They differ by the transformation of the adsorbed NO species which has been considered according to a bimolecular reaction between one molecule of CO and one of NO, both adsorbed (step [9] in mechanism 1), or between two adsorbed NO molecules (steps [14] and [15] in mechanism 2) or a dissociation of NO adsorbed (steps [16] in mechanism 3). In mechanism 4, the transition of an end-on NO to a flat lying species (step [17]) is considered. Steps [9], [14], [15], [16], and [17] were assumed to be rate determining.

To derive the rate expressions that correspond to these mechanisms we also assumed: (i) fast adsorption equilibria and (ii) NO and CO to be the most abundant adsorbed species and, hence, that adsorbed N and O atoms are supposed very reactive. We did not considered the case where the recombination of two adsorbed N atoms would be rate determining because, as demonstrated by Belton *et al.* (29) on Rh (111), on the basis of the kinetic study of N_2 desorption on Rh (111) (30), this process should be very fast.

The following rate expressions were obtained:

$$r = k_9\Theta_{NO}\Theta_{CO} \quad \text{Mechanism 1} \quad [20]$$

$$r = (k_{14} + k_{15})\Theta_{NO}^2 \quad \text{Mechanism 2} \quad [21]$$

$$r = k_{16}\Theta_{NO}\Theta_v \quad \text{Mechanism 3} \quad [22]$$

$$r = k_{17}\Theta_{NO} \quad \text{Mechanism 4,} \quad [23]$$

where Θ_i represents the surface coverage for compound i and Θ_v represents the fraction of vacant adsorption sites. As can be seen in Table 7, these rate expressions can be expressed for each mechanism as a function of λ_{NO}, λ_{CO}, the adsorption equilibrium constants of NO and CO, k_n, and the rate constants of the rate-determining steps (Eqs. [24]–[27]). All the rate expressions can be linearized, and λ_{NO}, λ_{CO}, and k_n can be obtained from the slopes α_i and the intercepts β_i of the linear plots $\sqrt{P_{NO} \times P_{CO}/r}$, $P_{NO}/\sqrt{r}$, $\sqrt{P_{NO}/r}$, and P_{NO}/r vs P_{NO} and P_{CO}. Calculations were preferentially made using the results obtained with Pt/Cr_3C_2 which gave the lower apparent order in NO since an order in NO close to 1 on Pt/Al_2O_3 would lead to slight changes in the ratio P_{NO}/r, probably of the same order of magnitude as the uncertainties of the

TABLE 7

Rate Expressions for the CO + NO Reactions Calculated for Mechanisms 1 to 4

Mechanism	rds	Rate	Linearized expression of the rate
1	$CO^* + NO^* \xrightarrow{k_9}$ [24]	$r = \frac{k_9 \lambda_{NO} \lambda_{CO} P_{NO} P_{CO}}{(1+\lambda_{CO} P_{CO} + \lambda_{NO} P_{NO})^2}$	$\sqrt{\frac{P_{NO} P_{CO}}{r}} = \frac{1+\lambda_{CO} P_{CO} \lambda_{NO} P_{NO}}{\sqrt{k_9 \lambda_{NO} \lambda_{CO}}}$
2	$2NO^* \xrightarrow{k_{14}}$ [25] $2NO^* \xrightarrow{k_{15}}$	$r = (k_{14} + k_{15}) \left[\frac{\lambda_{NO} P_{NO}}{(1+\lambda_{CO} P_{CO} + \lambda_{NO} P_{NO}} \right]^2$	$\frac{P_{NO}}{\sqrt{r}} = \frac{1+\lambda_{CO} P_{CO} + \lambda_{NO} P_{NO}}{\lambda_{NO} \sqrt{k_{14} + k_{15}}}$
3	$NO^* + * \xrightarrow{k_{16}}$ [26]	$r = \frac{k_{16} \lambda_{NO} P_{NO}}{(1+\lambda_{CO} P_{CO} + \lambda_{NO} P_{NO})^2}$	$\sqrt{\frac{P_{NO}}{r}} = \frac{1+\lambda_{NO} P_{NO} + \lambda_{CO} P_{CO}}{\sqrt{k_{16} \lambda_{NO}}}$
4	$NO^* \xrightarrow{k_{17}}$ [27]	$r = \frac{k_{17} \lambda_{NO} P_{NO}}{1+\lambda_{CO} P_{CO} + \lambda_{NO} P_{NO}}$	$\frac{P_{NO}}{r} = \frac{1+\lambda_{NO} P_{NO} + \lambda_{CO} P_{CO}}{k_{17} \lambda_{NO}}$

calculation and, hence, to inconclusive results. Moreover, as mentioned above, the lower deactivation of Pt/Cr_3C_2 probably leads to more accurate conversion measurements. The results obtained for Pt/Cr_3C_2 are reported in Table 8.

Clearly, mechanisms 1, 2, and 4 fail to describe the NO and CO dependence of the reaction rate since they lead to negative values for λ_{NO} and λ_{CO}. Only mechanism 3 gives realistic values for the three parameters.

The values for k_{16}, λ_{NO}, and λ_{CO} on Pt/Al_2O_3 and Pt/Si_3N_4, obtained using the same procedure, are listed in Table 9.

The experimental data have also been submitted to a mathematical method carried out from the solver setup of Excel 5. The criterion γ represents the summation of the square deviations between experimental and calculated rates:

$$\gamma = \sum_{i=1}^{n} (r_{i,\text{exp.}} - r_{i,\text{calc.}})^2. \qquad [28]$$

The adjustment of the unknown kinetic parameters is carried out by minimizing γ. The results are listed in Table 9.

TABLE 8

Rates and Adsorption Equilibrium Constants for the CO + NO Reaction over Pt/Cr_3C_2

Mechanism	α_i[a] i=CO	α_i[a] i=NO	β_i[b] i=CO	β_i[b] i=NO	λ_{NO} (atm^{-1})	λ_{CO} (atm^{-1})	k_n (mol g^{-1} h^{-1})
1	95.7	32.2	4.1×10^{-2}	0.36	−272	−808	
					−268	−798	
2	38	83.0	0.33	0.10	−976	−447	
					−976	−447	
3	537	456.0	4.7	5.09	188	222	9.1×10^{-4}
					190	223	9.1×10^{-4}
4	9113	5915	8.52	24.7	−281	−433	
					−283	−437	

[a] Slope of the linear plots $\sqrt{P_{NO} P_{CO}/r}$, $P_{NO}/\sqrt{r}$, $\sqrt{P_{NO}/r}$, P_{NO}/r vs P_{NO} and P_{CO}.

[b] Intercept of the linear plots $\sqrt{P_{NO} P_{CO}/r}$, $P_{NO}/\sqrt{r}$, $\sqrt{P_{NO}/r}$, P_{NO}/r vs P_{NO} and P_{CO}.

The parameter values obtained by the graphic method and by optimization are quite similar, taking the accuracy of the measurements into account. Moreover, Fig. 6, where the calculated rates obtained with the optimized values are plotted against the experimental rate, shows a good correlation between the two sets of rates. Concluding this part of the discussion, we find that of the four mechanisms that have been considered, mechanism 3 is the only one in agreement with the kinetic results obtained on the three platinum catalysts. Such a mechanism was already proposed on Pt/SiO_2 (18) and more recently over various noble metal catalysts (31, 32) by many investigators. However, only a few of them discussed the changes in the intrinsic properties of noble-metal-based catalysts for the CO + NO reaction from the quantitative evaluation of kinetic and thermodynamic constants. The following discussion will attempt to explain changes in Pt/Al_2O_3, Pt/Si_3N_4, and Pt/Cr_3C_2 activities by comparing the values of k_{16}, λ_{NO}, and λ_{CO} on the three catalysts.

The discussion of the values of k_{16} for the three catalysts is not easy. The NO dissociation rate constant (expressed per g catalyst) is significantly higher on Pt/Al_2O_3 than on the two other catalysts (about one order of magnitude). However, the Pt dispersion is substantially higher on Pt/Al_2O_3 than on Pt/Si_3N_4 and Pt/Cr_3C_2. Hence, the

TABLE 9

Constants for CO and NO over Pt at 300°C

Catalyst		λ_{CO} (atm^{-1})	λ_{NO} (atm^{-1})	k_{16}[a] (mol g^{-1} h^{-1})
Pt/Al_2O_3	[b]	127	15	8.9×10^{-3}
	[c]	121	11	11.4×10^{-3}
Pt/Si_3N_4	[b]	62	40	1.32×10^{-3}
	[c]	61	45	1.23×10^{-3}
Pt/Cr_3C_2	[b]	222	189	0.91×10^{-3}
	[c]	222	158	0.99×10^{-3}

[a] k_{16}: NO dissociation rate constant.

[b] Calculation by the graphic method.

[c] Calculation by the optimization method.

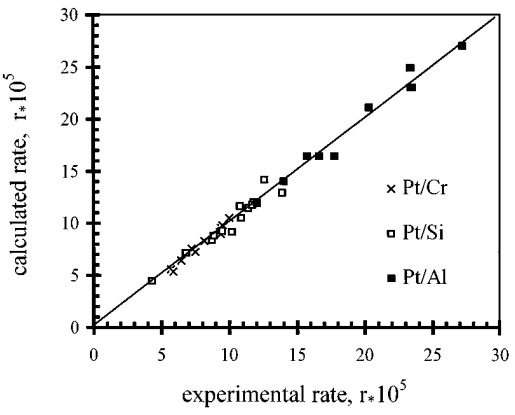

FIG. 6. Correlation between the experimental rates measured on Pt catalysts at 300°C and the calculated rates using the optimization method.

differences in the intrinsic rate constants, k'_{16}, (per m^2 Pt) are certainly different from those between the specific rate constants (per g catalyst). It can even be envisaged that k'_{16}, expressed per m^2 Pt or per Pt surface atom, may be higher on Pt/Si_3N_4 and Pt/Cr_3C_2 than on Pt/Al_2O_3, considering the d_{Pt} values obtained from the XPS analysis. However, since it has not been possible to measure the Pt surface area for Pt/Si_3N_4 and Pt/Cr_3C_2 because of the low hydrogen adsorption, it is not possible to calculate the intrinsic rate values of k'_{16}, which is the only way to obtain a good comparison of the properties of a catalyst.

Concerning the values of the adsorption equilibrium constants λ_{NO} and λ_{CO}, they change very much from one catalyst to another. The comparison of the values of λ_{NO} and λ_{CO} allows us to establish the following sequences:

$$Pt/Al_2O_3 < Pt/Si_3N_4 < Pt/Cr_3C_2 \quad \text{for } \lambda_{NO}$$

and

$$Pt/Si_3N_4 < Pt/Al_2O_3 < Pt/Cr_3C_2 \quad \text{for } \lambda_{CO}.$$

Consequently, the support seems to have a noticeable effect on the adsorption properties of platinum. Unfortunately, it is difficult to conclude that the support has an actual effect which modifies the electronic properties of Pt, or that a change in the metal particle size occurs, leading to a modification of the adsorptive and catalytic properties. From the selected rate expression, one can determine when the rate of CO oxidation by NO will be optimal by equating the derivative of r versus λ_{NO} to zero. This leads to the following equation:

$$\lambda_{NO} = \frac{1}{P_{NO}} + \lambda_{CO}\frac{P_{CO}}{P_{NO}}. \qquad [29]$$

Taking the pressure range conditions into account, where P_{NO} is usually low and always smaller than P_{CO}, the reaction rate will be optimal when λ_{NO} is substantially higher than λ_{CO}. Hence the optimization of the catalyst activity requires the following conditions for the adsorption properties : i) λ_{CO} should be as low as possible (it only appears at the denominator of the rate law); ii) values should be high for λ_{NO} but not too high in order to avoid an inhibiting effect, of NO; the difference between λ_{NO} and λ_{CO} should be as large as possible. Pt/Si_3N_4 provides the most interesting adsorption properties for the reaction CO + NO. Unfortunately the low specific surface area of Si_3N_4 (12.5 $m^2\ g^{-1}$) limits the dispersion of platinum to low values compared to those obtained with Al_2O_3 (100 $m^2\ g^{-1}$). Consequently the overall activity of Pt/Si_3N_4 is lower than that of Pt/Al_2O_3. A higher dispersion could be expected by using Si_3N_4 with a higher specific surface area which could further improve the Pt activity in the CO + NO reaction.

Returning to the values of the rate constant for NO dissociation and considering the estimation of the metal particle size based on XPS intensity measurements (Table 1), it is not unreasonable to assume that the intrinsic NO dissociation rate constants k'_{16} vary in accordance with the sequence $Pt/Cr_3C_2 > Pt/Si_3N_4 > Pt/Al_2O_3$, which is the same order obtained for λ_{NO}. Such a direct relationship between k'_{16} and λ_{NO} may well be explained by an interpretation based on the work of Blyholder (33) on the absorption frequency of CO adsorbed on metals. Backdonation of *d* electrons of the metal (*M*) to the π^* antibonding molecular orbitals in NO molecules would increase the strength of NO adsorption and weaken the N–O bond, which would further facilitate the dissociation of NO. Hence, changes in the k'_{16} and λ_{NO} values may be connected to a modification in the electronic properties of Pt. From these results, however, it does not seem possible to determine whether such a change is the result of direct metal support interactions or of changes in the size or structure of Pt particles. The reaction may simply be "structure sensitive." As a matter of fact, surface studies have shown that low index planes, such as Pt (111) (34) and Pt (110) (35), are inactive and do not dissociate NO contrary to Pt (100) (36) and Pt (410) (37). Banholzer *et al.* (38) proposed a model based on the Woodward–Hoffmann rules. This simple model can be regarded as a guideline for the structure sensitivity of N–O bond breaking. Hence, changes in the ability of platinum to dissociate NO would depend on the symmetry of these different MOs. Such conditions would imply a correct arrangement of surface atoms for NO bond breaking. Banholzer *et al.* (38) suggest that the transition $M \rightarrow \pi^*$ is symmetry forbidden on (111) and (110) surfaces. Our result would be consistent with the prediction model proposed by these authors if the orbital symmetry of the adsorption sites were modified by the nature of the support or by the metal particle size.

2.4. NO Reduction

The selectivity for N_2O formation (S_{N_2O}) is given by Eq. [30], where r_{N_2} represents the NO reduction rate into

N_2 and r_{N_2O} represents that into N_2O:

$$S_{N_2O} = \frac{r_{N_2O}}{(r_{N_2} + r_{N_2O})}. \quad [30]$$

As seen in Tables 3 to 5, changes in the r_{N_2}/r_{N_2O} ratio occur when P_{NO} varies, but to a lesser extent on Pt/Al_2O_3 than on Pt/Si_3N_4 and Pt/Cr_3C_2, under the partial pressure range conditions. According to Eq. [31], the overall transformation rate of NO is dependent on both the rate of CO oxidation by NO, r, and the ratio r_{N_2}/r_{N_2O}:

$$r_{NO} = r\left(1 + \frac{1}{1 + 2r_{N_2}/r_{N_2O}}\right). \quad [31]$$

From the rates of steps [10], [11], and [12] it is easy to establish (see Appendix II) the following relation between the rates of N_2 and N_2O formation

$$\frac{4r_{N_2}}{r_{N_2O}} + 1 = \frac{k_{11} + k_{12}}{k_{12}}\sqrt{1 + \frac{16k_{10}k_{16}}{k_{12}^2\lambda_{NO}P_{NO}}} + \frac{3k_{11}}{k_{12}}, \quad [32]$$

where k_{10} and k_{11} are the rate constants of N_2 formation according to steps [10] and [11], respectively, and k_{12} is the rate constant of the N_2O, step [12].

If k_{11} is negligible in comparison with k_{12} (as postulated by Lorimer and Bell (18)), which means that the bimolecular reaction between N_{ads} and NO_{ads} usually gives N_2O, then Eq. [32] can be simplified as

$$\left[\frac{4r_{N_2}}{r_{N_2O}} + 1\right]^2 = 1 + \frac{16k_{10}k_{16}}{k_{12}^2\lambda_{NO}P_{NO}}. \quad [33]$$

To check the validity of Eq. [33], the plots of $[4r_{N_2}/r_{N_2O} + 1]^2 - 1$ versus the reciprocal P_{NO} should give a straight line with a zero intercept. Such a relationship is indeed observed for Pt/Si_3N_4, Pt/Cr_3C_2 (Fig. 7). Hence, for these two catalysts, the formation of N_2 seems to occur mainly via the recombination of two adsorbed nitrogen atoms. The slopes of these straight lines equal to

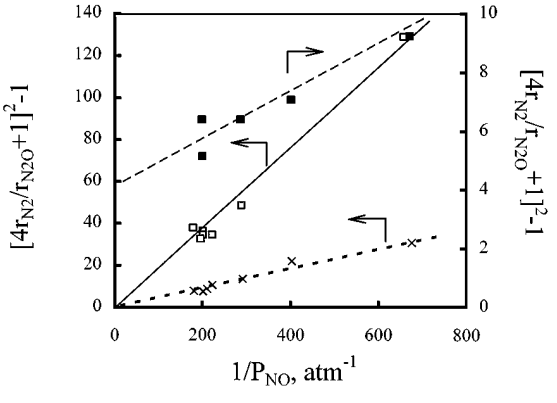

FIG. 7. Plots of $[4r_{N_2}/r_{N_2O} + 1]^2 - 1$ versus $1/P_{NO}$ on (×) Pt/Si_3N_4, (□) Pt/Cr_3C_2, and (■) Pt/Al_2O_3.

TABLE 10

Relative Rate Constants for the Formation of N_2 and N_2O over Pt Catalysts ($T = 300°C$, $P_{NO} = 1.5 \times 10^{-3}$ to 5.6×10^{-3} atm, $P_{CO} = 5 \times 10^{-3}$ atm)

Catalyst	Slope	Intercept	k_{10}/k_{12}^2	k_{11}/k_{12}
Pt/Cr_3C_2	0.15[a]	≅0[a]	2012	≅0
Pt/Si_3N_4	4.8×10^{-2} [a]	≅0[a]	91	≅0
Pt/Al_2O_3	3.8×10^{-4} [b]	0.30[b]	0.25	0.30

Note. k_{10}, k_{11}: rate constants for the formation of N_2 corresponding to the steps $2\,N^* \rightarrow N_2 + 2^*$ and $N^* + NO^* \rightarrow N_2 + O^* + ^*$, respectively k_{12}: rate constant for the formation of N_2O.

[a] From the plot of $[4(r_{N_2}/r_{N_2O}) + 1]^2 - 1$ vs $1/P_{NO}$.

[b] From the plot of r_{N_2}/r_{N_2O} vs $1/P_{NO}$.

$16k_{10}k_{16}/k_{12}^2\lambda_{NO}$ allow us to calculate the ratios k_{10}/k_{12}^2. The corresponding values are reported in Table 10.

On the contrary, a nearly straight line is obtained for Pt/Al_2O_3 but with a positive intercept (Fig. 7). Consequently, k_{11} is here not negligible in comparison with k_{12}. For this catalyst Eq. [32] should be used. But the fact that the plots of $[4r_{N_2}/r_{N_2O} + 1]^2$ vs $1/P_{NO}$ give a correct straight line implies that the expression $16k_{10}k_{16}/k_{12}^2\lambda_{NO}$ is probably small in comparison with k_{11}/k_{12}. In such a case it is easy to transform Eq. [32] into the expression

$$\frac{r_{N_2}}{r_{N_2O}} = \frac{k_{11}}{k_{12}} + 2\left[1 + \frac{k_{11}}{k_{12}}\right]\frac{k_{10}k_{16}}{k_{12}^2\lambda_{NO}P_{NO}}. \quad [34]$$

The slope and the intercept (3.85×10^{-4} and 0.30, respectively) of the linear plot r_{N_2}/r_{N_2O} vs $1/P_{NO}$ enable us to calculate k_{11}/k_{12} and k_{10}/k_{12}^2 for Pt/Al_2O_3 (Table 10).

Equation [32] gives the conditions for good selectivity. The selectivity of the CO + NO reaction for the formation of N_2 is enhanced when: (i) k_{10}, k_{11} are higher than k_{12}, (ii) the NO dissociation rate constant k_{16} is high, and (iii) λ_{NO} and P_{NO} are low. It can be seen that, despite a value of λ_{NO} increasing in the order $Pt/Al_2O_3 < Pt/Si_3N_4 < Pt/Cr_3C_2$, a reverse order for the selectivity r_{N_2}/r_{N_2O} is obtained because of a very high increase in the ratio k_{10}/k_{12}^2, i.e., an increase in the rate constant of recombination of the two adsorbed N atoms in comparison with that of the reaction $N_{ads} + NO_{ads}$.

Unfortunately it is not possible to check the effect of k_{16} (NO dissociation rate constant) on the selectivity of our catalysts since this rate constant varies proportionally to the number of Pt surface atoms, and, as already mentioned, the intrinsic rate constant, k'_{16} (expressed per metallic atom), cannot be calculated.

CONCLUSION

The aim of this study was to investigate the kinetics of NO and CO transformations over platinum-based catalysts. Four mechanism schemes, able to describe the reactions of

NO with CO, were considered. From activity and selectivity measurements we selected the mechanism scheme

$$CO + {}^* \Leftrightarrow CO^* \quad [7]$$

$$NO + {}^* \Leftrightarrow NO^* \quad [8]$$

$$NO^* + {}^* \rightarrow N^* + O^* \quad [16]$$

$$2N^* \rightarrow N_2 + 2^* \quad [10]$$

$$N^* + NO^* \rightarrow N_2 + O^* + {}^* \quad [11]$$

$$N^* + NO^* \rightarrow N_2O + 2^* \quad [12]$$

$$O^* + CO^* \rightarrow CO_2 + 2^*, \quad [13]$$

which is valid for Pt deposited on the three supports.

Assuming, first, fast competitive and nondissociative adsorptions of CO and NO and, second, the dissociation of NO adsorbed species on a vacant nearest neighbor site as rate determining, the following rate law expression is established:

$$r = \frac{k_{16}\lambda_{NO}P_{NO}}{(1 + \lambda_{CO}P_{CO} + \lambda_{NO}P_{NO})^2}.$$

The NO dissociation rate constant (k_{16}) and the reactant equilibrium constants of adsorption (λ_{NO}, λ_{CO}) were calculated using both graphic and statistical methods. The equilibrium constant of NO adsorption is considerably lower than that of CO (15 against 127 atm^{-1}) on Pt/Al_2O_3, which explains very well the poor performances of this catalyst in the CO + NO reactions. It has been clearly shown that a change in the support leads to large changes in the platinum adsorption properties. First, the strength of CO adsorption is notably lower on Pt/Si_3N_4 than on Pt/Cr_3C_2 and Pt/Al_2O_3. On the contrary, NO adsorption notably increases when platinum is deposited on Si_3N_4 and still more on Cr_3C_2.

The low value of λ_{CO} on Pt/Si_3N_4, associated with a value of the difference of $\lambda_{NO} - \lambda_{CO}$ higher than those of the other catalysts, indicates that this catalyst exhibits for the oxidation of CO by NO the best adsorption properties among the three Pt catalysts discussed in the work. Unfortunately, the low Pt dispersion limits the overall rate of CO + NO.

The nature of the support also has a significant effect on the selectivity of NO transformation. Pt/Cr_3C_2 clearly gives the best selectivity for N_2 formation, before Pt/Si_3N_4 and then Pt/Al_2O_3. This seems to be related mainly to the fact that the recombination of two adsorbed N atoms is very much favored in comparison with the reaction between one adsorbed N atom and one adsorbed NO molecule. The reverse situation is observed on Pt/Al_2O_3. Hence, Pt supported on Cr_3C_2 and on Si_3N_4 exhibit interesting catalytic properties to convert NO and CO. Nevertheless, despite the promising performance of Pt/Cr_3C_2, further developments on an industrial scale are limited because of the high toxicity of chromium. On the contrary, keeping in mind its resistance to oxidation and its good adsorption properties for NO, Si_3N_4 with higher surface specific areas, it seems promising as a new support for metals in TWCs.

APPENDIX I: ESTIMATION OF THE Pt PARTICLE SIZE FROM XPS

These calculations were based on the simple model of cubic Pt particles (edge, d_{Pt}) deposited on a nonporous support as described, for example, in Ref. (15).

The ratio of XPS intensities is

$$\frac{I_{Pt}}{I_S} = f_{Pt}\left[\frac{n_{Pt}}{n_S}\right]\left[\frac{T(E_{kinet.,Pt})}{T(E_{kinet.,S})}\right]\left[\frac{\sigma_{Pt}}{\sigma_S}\right]\left[\frac{\lambda_{Pt\rightarrow Pt}}{\lambda_{S\rightarrow S}}\right] \times \left[\frac{1 - \exp\left(-\frac{d_{Pt}}{\lambda_{Pt\rightarrow Pt}}\right)}{(1 - f_{Pt}) + f_{Pt} \times \exp\left(-\frac{d_{Pt}}{\lambda_{S\rightarrow Pt}}\right)}\right], \quad [35]$$

where f_{Pt} is the fraction of the support covered with Pt, n_{Pt}, and n_S are the densities of Pt atoms and of the metal atoms of the support (Al, Si, Cr), σ are the cross sections, T is the transmission factor of the spectrometer (T is proportional to the kinetic energy $E_{kinet.}$ of the photoelectrons corresponding to the levels considered), $\lambda_{X\rightarrow Y}$ is the mean path of the electron emitted by the element X in a matrix Y, and d_{Pt} is the particle size of Pt.

The levels considered were Pt 4*f* for Pt/Si_3N_4 and Pt/Cr_3C_2, Pt 4*d* for Pt/Al_2O_3, Al 2*p*, Si 2*p*, and Cr 2*p*.

The values of the cross sections σ were found in Ref. (39). Those of λ_S were estimated according to Ref. (40) by using the equations

$$\lambda(\text{nm}) \cong 0.41a(aE_{kinet.})^{0.5} \quad \text{for simple elements} \quad [36]$$

$$\lambda(\text{nm}) \cong 0.72a(aE_{kinet.})^{0.5} \quad \text{for inorganic compounds} \quad [37]$$

with

$$a^3(\text{nm}^3) = \frac{10^{24}A}{\rho n N}, \quad [38]$$

where A is the atomic or molar mass (g mol^{-1}) of the compound, n is the number of atoms in the molecule, ρ is the density, and N is Avogadro's number. The estimates for all the λ_S are close to each other. Hence, considering that the above expressions are only approximate, we considered that the ratios λ_{Pt}/λ_S are close to 1 with $\lambda_{Pt\rightarrow Pt} = 1.9$ nm.

One can easily calculate f_{Pt} according to

$$f_{Pt} = \frac{x}{\rho_{Pt} S d}, \quad [39]$$

where x is the Pt weight on 1 g catalyst, ρ_{Pt} is the Pt density, and S is the support specific surface area. The specific surface area of Cr_3C_2 was estimated to be 0.02 $m^2\,g^{-1}$ from its particle size of 45.9 μm assuming a sperical shape and a

nonporous material. The values obtained for the Pt particle sizes are listed in Table 1.

APPENDIX II

The overall rate of N_2 formation takes into account the contribution of the two competitive processes [10] and [11]

$$r_{N_2} = k_{10}\Theta_N^2 + k_{11}\Theta_N\Theta_{NO} \quad [40]$$

and the reaction rate for the formation of N_2O, according to the reaction step [12], is given by

$$r_{N_2O} = k_{12}\Theta_N\Theta_{NO}. \quad [41]$$

One can express the ratio r_{N_2}/r_{N_2O}:

$$\frac{r_{N_2}}{r_{N_2O}} = \left(\frac{k_{10}}{k_{12}}\frac{\Theta_N}{\Theta_{NO}}\right) + \frac{k_{11}}{k_{12}}. \quad [42]$$

Θ_N and Θ_{NO} can be calculated by applying the quasi-steady-state approximation to N adsorbed species:

$$\frac{d\Theta_N}{dt} = k_{16}\Theta_{NO}\Theta_V - k_{10}\Theta_N^2 - \left(\frac{k_{11}+k_{12}}{2}\right)\Theta_{NO}\Theta_N \cong 0. \quad [43]$$

From Eq. [43] we can extract the ratio Θ_N/Θ_{NO}:

$$\frac{\Theta_N}{\Theta_{NO}} = \frac{(k_{11}+k_{12})}{4k_{10}}\left[-1+\sqrt{1+\frac{16k_{10}k_{16}}{(k_{11}+k_{12})^2\lambda_{NO}P_{NO}}}\right]. \quad [44]$$

Equation [44] is then introduced into Eq. [42] which after rearrangement leads to

$$\frac{4r_{N_2}}{r_{N_2O}} + 1 = \frac{k_{11}+k_{12}}{k_{12}}\sqrt{1+\frac{16k_{10}k_{16}}{k_{12}^2\lambda_{NO}P_{NO}}} + \frac{3k_{11}}{k_{12}}. \quad [32]$$

ACKNOWLEDGMENT

This work was supported by a grant from the "Groupement de Recherche sur les Pots Catalytiques," initiated by the CNRS and the Institut Français du Pétrole.

REFERENCES

1. Shelef, M., and Graham, G. W., *Catal. Rev. Sci. Eng.* **36**, 433 (1994).
2. Taylor, K. C., *Catal. Rev. Sci. Eng.* **35**, 457 (1993).
3. Masel, R. I., *Catal. Rev. Sci. Eng.* **28**, 335 (1986).
4. Taylor, K. C., *Chemtech.* **20**, 551 (1990).
5. Gandhi, H. S., Yao, H. C., and Stepien, H. K., *in* "ACS Symp. Ser.," No. 178 (A. T. Bell and L. Hegedus, Eds.), p. 143, 1982.
6. Plummer, H. K., Jr., Schinozaki, S., Adams, K. M., and Gandhi, H. S., *J. Molec. Catal.* **20**, 251 (1983).
7. Leclercq, G., Dathy, C., Lamonier, J. F., Mabilon, G., Prigent, M., and Leclercq, L., *in* "Three Way Automotive Catalysis—Fundamental Approach to Precious Metal Catalysts Preparation and Aging—Reaction Mechanisms, Kinetics and Modeling" (G. Mabilon and M. Prigent, Eds.), Chapter 8, Technip, in press.
8. Dathy, C., Thesis, Lille 1993.
9. Ng, K. Y. S., Belton, D. N., Schmieg, S. J., and Fisher, G. B., *J. Catal.* **146**, 394 (1994).
10. Oh, S. H., and Eickel, C. C., *J. Catal.* **128**, 526 (1991).
11. Leclercq, G., and Boudart, M., *J. Catal.* **71**, 127 (1981).
12. Leclercq, G., Leclercq, L., and Maurel, R., *Bull. Soc. Chim. Fr.* 2329 (1974).
13. Leclercq, G., Leclercq, L., and Maurel, R., *J. Catal.* **44**, 68 (1976).
14. Wagner, C. D., Riggs, W. M., Davis, L. E., and Moulder, J. F., "Hand Book of X-Ray, Photoelectron Spectroscopy" (G. E. Muilenberg, Ed.), Perkin–Elmer, Palo Alto, CA, 1979.
15. Grimblot, J., *in* "Analyse des surfaces des solides" (Masson, Ed.), p. 125, 1995.
16. Fung, S. C., *J. Catal.* **58**, 454 (1979).
17. Cho, B. K., Shanks, B. H., and Bailey, J. E., *J. Catal.* **115**, 486 (1989).
18. Lorimer, D., and Bell, A. T., *J. Catal.* **59**, 223 (1979).
19. Mergler, Y. J., and Nieuwenhuys, B. E., *J. Catal.* **161**, 292 (1996).
20. Alikina, G. M., Davydov, A. A., Sazanova, I. S., and Popovskii, V. V., *React. Kinet. Catal. Lett.* **27**, 279 (1985).
21. Oh, S. H., and Carpenter, J. E., *J. Catal.* **101**, 114 (1986).
22. Permana, H., Ng, K. Y. S., Peden, C. H. F., Schmieg, S. J., and Belton, D. N., *J. Phys. Chem.* **99**, 16344 (1995).
23. Baure, B. A., Wickham, D. T., and Koel, B. E., *J. Catal.* **119**, 238 (1989).
24. Taylor, K. C., and Schlatter, J. C., *J. Catal.* **63**, 53 (1980).
25. Aldock, W., and Linz, H. G., *Surf. Sci.* **46**, 61 (1974).
26. Klein, R. L., Schwartz, S. B., and Schmidt, L. D., *J. Phys. Chem.* **89**, 4908 (1985).
27. Kudo, A., Steinberg, M., Bard, A. J., Campion, A., Fox, M. A., Mallouk, T. E., Weber, S. E., and White, J. M., *J. Catal.* **125**, 565 (1990).
28. Hecker, W. C., and Bell, A. T., *J. Catal.* **84**, 200 (1983).
29. Belton, D. N., and Schmieg, S. J., *J. Catal.* **144**, 9 (1993).
30. Belton, D. N., DiMaggio, C. L., and Ng, K. Y. S., *J. Catal.* **144**, 273 (1993).
31. Cho, B. K., *J. Catal.* **138**, 255 (1992).
32. Oh, S. H., Fisher, G. B., Carpenter, J. E., and Goodman, D.W., *J. Catal.* **100**, 360 (1986).
33. Blyholder, G., *J. Phys. Chem.* **68**, 2772 (1964).
34. Gland, J. L., and Sexton, B. A., *Surf. Sci.* **94**, 355 (1980).
35. Gorte, R. J., and Gland, J. L., *Surf. Sci.* **102**, 348 (1981).
36. Fisher, T. E., and Kelemen, S. R., *J. Catal.* **53**, 24 (1978).
37. Banholzer, W. F., and Masel, R. I., *J. Catal.* **85**, 127 (1984).
38. Banholzer, W. F., Park, Y. O., Mak, K. M., and Masel, R. I., *Surf. Sci.* **128**, 176 (1983).
39. Scofield, J. H., *J. Electron Spectrosc. Related Phenom.* **8**, 129 (1976).
40. Seah, M. P., and Dench, W. A., *Surf. Interface Anal.* **1**, 2 (1979).